

The Ion Propulsion System on NASA's Space Technology 4/Champollion Comet Rendezvous Mission

John R. Brophy, Charles E. Garner, James E. Polk, and Jeffery M. Weiss.
*Jet Propulsion Laboratory
 California Institute of Technology
 Pasadena, California*

The ST4/Champollion mission is designed to rendezvous with and land on the comet Tempel 1 and return data from the first-ever sampling of a comet surface. Ion propulsion is an enabling technology for this mission. The ion propulsion system on ST4 consists of three ion engines each essentially identical to the single engine that flew on the DS1 spacecraft. The ST4 propulsion system will operate at a maximum input power of 7.5 kW (3.4 times greater than that demonstrated on DS1), will produce a maximum thrust of 276 mN, and will provide a total ΔV of 11.4 km/s. To accomplish this the propulsion system will carry 385 kg of xenon. All three engines will be operated simultaneously for the first 168 days of the mission. The nominal mission requires that each engine be capable of processing 118 kg. If one engine fails after 168 days, the remaining two engines can perform the mission, but must be capable of processing 160 kg of xenon, or twice the original thruster design requirement. Detailed analyses of the thruster wear-out failure modes coupled with experience from long-duration engine tests indicate that the thrusters have a high probability of meeting the 160-kg throughput requirement.

Introduction

Space Technology 4 (ST4)/Champollion is the fourth mission in NASA's New Millennium program. The first mission in this series was Deep Space 1 (DS1) which was launched in October, 1998 and demonstrated, for the first time, the use of ion propulsion as the primary propulsion system for a deep-space mission. The objectives for ST4/Champollion are to flight validate technologies, systems and procedures necessary for rendezvous, landing and anchoring a science payload on a comet [1]. In addition, this mission seeks to acquire science data on the properties, composition and morphology of a comet while performing the first-ever sampling and analysis of the surface and subsurface. In situ investigation of a cometary nucleus is expected to provide key data for understanding the origin of the solar system. ST4 is scheduled for an April 2003 launch using a Delta II 7925 and will arrive at the comet Tempel 1 approximately three years later.

The heliocentric ΔV required to catch up to and rendezvous with the comet will be provided by a multi-engine solar electric propulsion (SEP) system based on

the single-ion-engine system used on DS1. The ST4 multi-engine SEP system is a technology applicable to many other deep-space missions of interest including Mercury Orbiter, Neptune Orbiter, Titan Explorer, Saturn Ring Observer, Europa Lander, Comet Sample Return, and Venus Sample Return, as well as to a variety of near-Earth-space missions. Electric power for the SEP system and the spacecraft will be provided by an advanced a 10-kW (beginning-of-life at 1 AU) solar array having a specific mass of approximately 10 kg/kW.

Why Ion Propulsion for ST4?

The use of ion propulsion for comet rendezvous missions is a dream that has long fascinated mission planners and electric propulsion technologists alike. Serious mission and system studies for comet rendezvous missions began in the 1960's (see for example Refs. 2-4) following the successful operation of the first broad-beam, electron-bombardment ion engine in the laboratory at NASA's Lewis Research Center (now the Glenn Research Center) in 1960 [5]. Numerous comet rendezvous mission studies based on

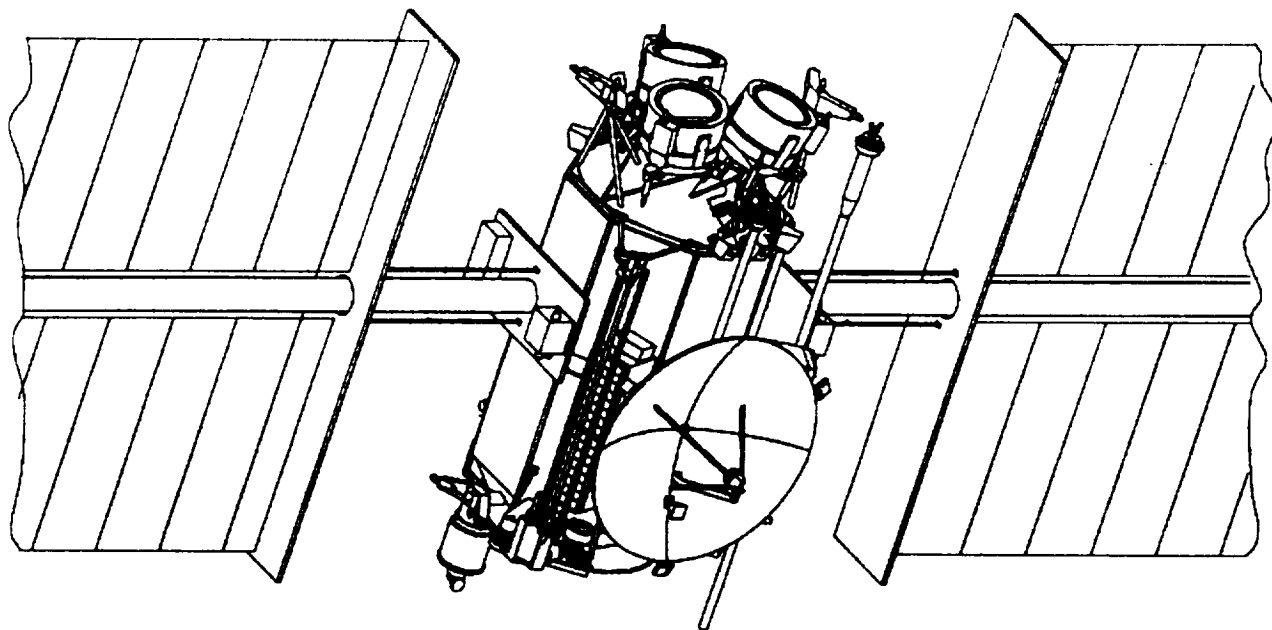


Fig. 1 ST4 spacecraft in the cruise configuration.

an advanced xenon feed system. Each ion engine is attached to a two-axis gimbal mechanism capable of pointing the thruster ± 10 degrees in each axis. The propulsion system is controlled by only one DCIU at a time, the other DCIU is maintained as a cold spare. The PPU's are cross-strapped so that each PPU can operate either of two engines, and each engine is attached to two PPU's. This cross-strapping capability was designed into the NSTAR PPU's in anticipation of this type of configuration.

The advanced xenon feed system replaces the bang-bang pressure regulation system used on DS1 with active pressure regulators based on new components currently under development. Candidates for the pressure regulator include the multifunction valve from Marotta Scientific Controls, Inc. and the proportional solenoid valve from Moog, Inc. The use of these new components enables the elimination of the relatively large and heavy plenum tanks used in the DS1 XFS.

The mass breakdown of the ion propulsion system is given in Table 1. This mass list does not include the masses for the gimbals, the wire harnesses, or the thermal control hardware, all of which are book-kept with other spacecraft subsystems.

Table 1 ST4 IPS Mass List

Component	Qty	Unit Mass (kg)	Total Mass (kg)	Mass Cont. (kg)
Ion Engine	3	8.34	25.02	3.75
PPU	3	14.82	44.46	6.67
DCIU	2	2.80	5.60	1.40
XFS	1	9.34	9.34	2.75
Tank	1	13.80	13.80	3.40
Total			98.22	

The power from the solar array as a function of time into the ST4 mission is given in Fig. 2. The variation in power is due to the changing spacecraft distance from the sun and accounts for the variation in solar cell efficiency with temperature and the effects of radiation damage. The lower curve in this figure is the total power input to the ion propulsion system. The difference between these curves is the power available to the rest of the spacecraft.

The trajectory for ST4 requires that all three of the ion engines operate simultaneously for approximately the first six months of the mission. After the first six months no more than two engines are operated at the

Two possible mechanisms have been identified to date in which multiple engine operation may impact the engine life. The first of these is the effect on the accelerator grid impingement current. Multiple engine operation will generate more charge-exchange ions than a single engine and it is not known if this will impact the magnitude or distribution of the currents collected by each engine's accelerator grid. If the magnitude increases or the distribution changes, the service life of the accelerator grid could be impacted.

The second mechanism concerns the non-uniform heating of one thruster due to the operation of an adjacent thruster. This non-uniform heating will change the thermal expansion of the thruster possibly impacting the containment of thin sputter-deposited films. Since the behavior of these thin films is not well understood, the degree to which this is a problem cannot be quantified. It should be noted, however, that varying sun angles on a spacecraft with a single ion engine will also result in asymmetric heating of the thruster.

Finally, for multiple engine operation the DCIU must startup, control, and shutdown any combination of the three engines on ST4. The software in the NSTAR DCIU was designed to handle multiple thruster operation, but this feature could not be tested with the single-thruster system on DS1. There appears to be value in testing the DCIU software with multiple PPU's operating multiple real thrusters. Real thrusters, instead of resistive loads, are believed to be necessary to assess potential timing issues and the ability of the DCIU to handle off-nominal conditions.

Engine Throughput Requirement

From the trajectory analyses a total 350 kg of xenon is required to perform this mission. Currently a 10% contingency on the propellant mass is being carried for a total propellant loading of 385 kg. The amount of propellant processed by each engine is given in Fig. 4 vs. mission time. These data indicate that each thruster must process approximately 118 kg of xenon. The NSTAR program has as one of its remaining objectives to demonstrate a total propellant throughput capability per engine of 125 kg. This demonstration is taking place in an on-going Extended Lifetime Test (ELT) at JPL. As of the end of May the thruster had successfully processed approximately 43 kg of xenon. Further details regarding this test are provided by Anderson [33].

The upper curve in Fig. 4 represents the amount of propellant each thruster would have to process if one

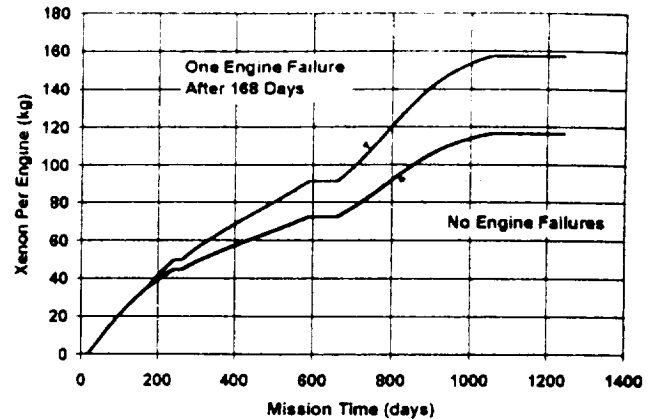


Fig. 4 Throughput required per engine for the ST4 mission.

thruster were to fail six months into the mission (after there is no longer the requirement to operate three thrusters simultaneously). In this case, the remaining thrusters must process a total of nearly 160 kg of xenon each. This is twice the original design goal for the NSTAR thruster. A total throughput of 160 kg is approximately equal to 16,000 hours of operation at full power.

The throughput requirement per thruster could be mitigated by simply adding a fourth thruster to the propulsion system. If this were done the nominal throughput requirement, assuming no thruster failures would be 88 kg per engine. In the case where one thruster fails at the beginning of the mission, the throughput requirement for the remaining thrusters is the same as the current ST4 design with no thruster failures, i.e., 118 kg. The addition of a fourth thruster, however, is not an attractive option because it would result in a significant increase in the mass of the ion propulsion system. This mass increase is the result of the added thruster mass, as well as the mass of another gimbal, additional feed system components, an additional wiring harness, and additional miscellaneous structure. The resulting mass growth of the propulsion system would severely impact the mass budgets the other spacecraft subsystems. Consequently, the ST4 program is strongly motivated to be able to fly with only three ion engines. The critical question is whether the NSTAR ion engines have sufficient throughput capability to perform this mission.

Engine Throughput Capability

NSTAR included as an integral part of the program a task to assess the service life capability of the ion

Screen Grid Structural Failure. Structural failure of the screen grid by ion sputtering has been treated probabilistically [38]. Most of the erosion damage to the screen grid is believed to be caused by multiply charged ions produced in the discharge chamber. Consequently, this failure mode is very sensitive to the ratio of double to single ion production rates, as well as to the potential difference between the screen grid and the discharge chamber plasma. The time to failure of the screen grid is given in [38] as,

$$T_{sg} = \frac{t_s \phi_i f_b e \rho A_b (1 - \phi_s) (1 + f_d R_{+}^{++})}{J_b m_g (1 - \phi_i) \left(Y_{+} + \frac{f_d}{2} R_{+}^{++} Y_{++} \right)} \quad (1)$$

which simply describes the time required to sputter-erode completely through the screen grid on the centerline of the thruster. All of the symbols in Eq. (1) are defined in Table 2. Also listed in this table are the ranges for each parameter that cannot be specified exactly. The uncertainty in the values of these key parameters is handled probabilistically using a Monte Carlo simulation. A value for each parameter is selected at random from within its allowable range of values. The time to screen grid structural failure, T_{sg} , is then calculated from Eq. (1). The process is repeated typically 100,000 times. Because the values of the input parameters vary, the calculated failure times will form a distribution. This analysis indicates that the peak in the failure distribution shown in Fig. 5 occurs at approximately 27,000 hours of operation at full power. Normalizing this distribution and then integrating over different run times results in the curve of the failure probability versus run time given in Fig. 6. This figure suggests that there is less than 1 chance in 1000 that the screen grid will fail after 16,000 hours of operation at full power, which is equivalent to a throughput of 160 kg.

These calculations assume that all of the xenon is processed at the engine's full power point, an assumption which significantly simplifies the calculations. In reality the engines will be run over the throttling curve given in Fig. 3. It can be shown using Eq. (1), however, that the full power point is the most stressing case. That is, from the standpoint of screen grid failure, the total engine throughput capability is smallest when operated at full power. Therefore, the failure risk curve in Fig. 6 is conservative.

Another major source of uncertainty in this analysis comes from the low-energy sputter-yield values used to

Table 2 Parameters for Eq. (1)

Symbol	Definition	Values
A_b	Active grid area [m ²]	0.06587
e	Electron charge [coul.]	1.6×10^{-19}
f_b	Beam current flatness parameter	0.40 to 0.46
f_d	Double ion ratio correction to centerline parameter	1.40 to 1.67
J_b	Beam Current [A]	$1.76 \pm 1\%$
m_g	Mass of screen grid atom [kg]	1.59×10^{-25}
R_{+}^{++}	Measured double to single ion current ratio	0.15 to 0.20
t_s	Screen grid thickness [m]	3.80×10^{-4}
V_d	Discharge voltage [V]	24.5 to 26.0
Y_{+}	Single ion sputter yield = $1.06 \times 10^{-5} + (V_d - 24.8)^2$ [atoms/ion]	$\pm 50\%$
Y_{++}	Double ion sputter yield = $1.06 \times 10^{-5} + (2V_d - 24.8)^2$ [atoms/ion]	$\pm 50\%$
ρ	Density of screen grid material [kg/m ³]	10220
ϕ_i	Screen grid transparency to ions	0.82
ϕ_s	Screen grid open area fraction	0.67

determine the screen grid erosion rates. Since there is no sputter-yield data in the literature over the voltage range of interest (24 V to 60 V), an extrapolation of sputter-yield data obtained at higher energies to the energy range of interest was performed using an approach described by Rawlin [44]. Since extrapolations are inherently uncertain, an uncertainty of $\pm 50\%$ was added to the calculated sputter-yield values. There are activities currently underway to measure the sputter-yield of molybdenum at low energy, but these have not yet produced reliable data [45]. In the meantime the analysis of the screen grid erosion captures this lack of knowledge in the form of increased failure risk. Finally, it should be noted, that the screen grid, after the 8,000-hr test, showed very little erosion [42].

50 μm were found the conclusion of the 8,000-hr test [42]. These were by far the thickest material deposits found anywhere in the thruster. If this material flakes off, it could short the keeper to the cathode, making ignition of the cathode much less likely, or it could short the accelerator system electrodes with a material flake that may be too big to be cleared with the grid clearing circuit. At this time the maximum size of a molybdenum or tungsten flake that can be cleared by the grid clearing circuit is unknown, but there are plans for the NSTAR program to obtain this information. In addition, slight modifications to the keeper could be made to significantly improve the adherence of sputter-deposited material. For the thruster used in the 8,000-hr test this surface was not subjected to any kind of flake containment treatment since it was not recognized as a significant deposition site prior to the 8,000-hr test.

Hollow Cathode Life. The end of life for a hollow cathode will typically manifest itself as a failure to start. This will occur when there is insufficient low-work function material available at the emitter surface to provide enough free electrons at the cathode's ignition temperature to initiate breakdown of the xenon gas for the applied ignition voltage. Higher temperatures and higher ignition voltages facilitate cathode ignition. The cathode is engineered to establish an insert temperature typically between 1100°C and 1200°C for startup. The ignition voltage is limited to 650 V for the NSTAR engine because this voltage level has been shown to produce reliable cathode ignition in the Space Station Plasma Contactor development program. Higher voltages are possible, but come at the expense of increased complexity associated with handling the higher voltage level.

The longest duration test of a xenon hollow cathode on record is the 28,700-hr test performed by Sarver-Verhey [46, 47]. This cathode is the same diameter and uses the same insert as the NSTAR ion engine cathode, and was operated at an emission current of 12 A for the entire endurance test. The test was terminated when the cathode failed to start after 28,700 hours. Post-test analysis of the cathode confirmed that the cathode insert had reached the end of its service life [47]. This test demonstrated a total emitted charge capability of 334,000 A-hrs. Inspection of the test results, however, indicates that after 23,000 hours the cathode temperature started to rise rapidly [47]. In addition, the voltage required to ignite the cathode exceeded the 650-V capability of the NSTAR ignitor circuit at this time. Therefore, a more conservative estimate would

place the cathode end-of-life at 23,000 hours for a total charge transfer of 276,000 A-hrs.

The emission current for the NSTAR ion engine at full power changes as a function of time as the accelerator grid apertures enlarge due to ion sputtering. For the first 2,000 hours of the 8,000-hr test the discharge current was between 13 A and 14 A. Between 2,000 hrs and 4,000 hrs the discharge current increased to 15 A and the discharge current stayed roughly between 15.0 A and 15.5 A over the last 4,000 hours of the test [42]. In the ongoing ELT the discharge current at full power has increased slowly from about 14 A at 500 hours to 14.5 A at 4,300 hours [33]. The discharge current in the ELT is slightly lower than that in the 8,000-hr test because the discharge voltage is slightly higher. The higher discharge voltage is believed to be the result of the ELT flow rates being approximately 2% lower than in the 8,000-hr test. The higher discharge voltage will affect the screen grid life so there is a trade-off between screen grid life and cathode life.

The cathode emission current is the difference between the discharge current and the beam current. Assuming a constant discharge current of 15 A and a beam current of 1.76 A, the emission current is 13.2 A. If the total emitted charge capability of the cathode is given by the lower estimate of 276,000 A-hrs, then the cathode life is 20,800 hours for thruster operation at full power. If the higher value for total emitted charge capability is used, i.e., 334,000 A-hrs, then the cathode life is 25,000 hours. These estimates, unfortunately, are highly uncertain since the rate at which the low-work-function material gets depleted in the cathode is known to be a function of the insert temperature, and how the temperature of the insert for the cathode inside the NSTAR ion engine relates to the insert temperature for the cathode in the 28,700-hr test is unknown. The cathode thermal environment in Sarver-Verhey's test is substantially different than that inside the ion engine. Probabilistic modeling of the cathode life has not been performed so this uncertainty cannot currently be quantified.

Grid shorts. The relatively small separation between the screen and accelerator grids (approximately 0.6 mm) can easily be bridged by debris from many sources resulting in a grid short. For this reason the NSTAR PPU includes a grid-clearing circuit whose sole function is to remove this debris and re-establish the ability of the accelerator system to stand-off the total voltage applied between the grids. The grid-clearing circuit and its capabilities are described in

where the parameters and their values or ranges of values are defined in Table 3. The ranges given in this table represent the best current understanding of the possible values that each of these parameters can have. The parameters α and f_a , characterize the uncertainty in the erosion geometry. The spread in values given for these parameters is consistent with the variability observed in the NSTAR long-duration test program. The parameters β and λ_{pg} capture the uncertainty in the erosion rate in the pits and grooves pattern. For a given value of β , the value of λ_{pg} is selected from a range that depends on β so that the resulting erosion rates are also within the variability observed in the NSTAR long-duration tests. The intrinsic variability of these parameter is expected to be smaller than that represented in Table 3 so that these ranges will likely be reduced as more information is obtained.

Using Eq. (2) in the same probabilistic methodology described for the screen grid erosion characterized by Eq. (1) results in a B1 life (1 chance in 100 of failing) of about 22,000 hours for a fixed accelerator grid voltage of -180 V. If instead, the accelerator grid voltage is fixed at -250 V (the limit of the accelerator supply in the NSTAR PPU), then the B1 life is reduced to about 15,000 hours as indicated in Fig. 7.

Electron-backstreaming. Electron-backstreaming occurs when the accelerator grid can no longer prevent electrons in the beam plasma from traveling back into the positive-high-voltage engine. The magnitude of the negative voltage applied to the accelerator grid that is required to prevent electron-backstreaming is primarily

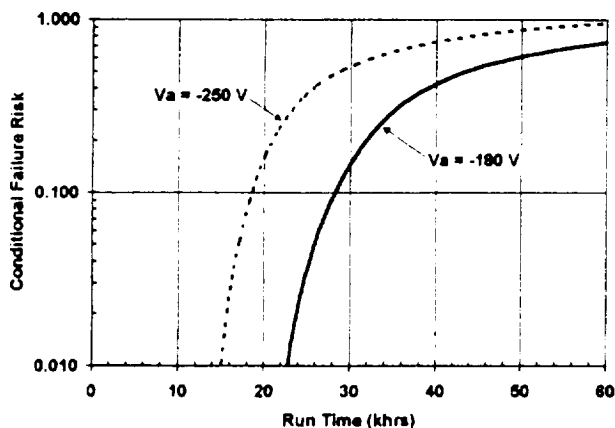


Fig. 7 Risks for accelerator grid structural failure with -180 V and -250 V on the accelerator grid.

a function of the positive high voltage, the thickness of the accelerator grid, the screen-accelerator grid separation, the ion current density, and the accelerator grid hole diameter.

Computer models can readily calculate the effects of these parameters on the local potential across the accelerator grid aperture. An axisymmetric code, written by K. Ishihara and Y. Arakawa of the University of Tokyo, provides a very simple tool to illustrate these effects. When using this code in this study, the onset of electron-backstreaming was defined, for a given geometry, as the smallest magnitude accelerator grid voltage which would result in no negative equipotential contours spanning the accelerator grid aperture. With no negative voltage contours spanning the grid aperture, there is no potential barrier to prevent the backstreaming of electrons. While this definition is probably not strictly correct, it is expected to be a reasonable approximation because the temperature of the electrons in the beam plasma is low (typically 1 or 2 eV).

Erosion of the accelerator grid apertures by ion sputtering during normal engine operation will increase the hole diameters as a function of run time. The effect of accelerator hole diameter increase on the electron-backstreaming voltage is given in Fig. 8 based on the Ishihara-Arakawa code. The calculations were made for an ion current density corresponding to a normalized perveance per hole of $2.1 \times 10^{-9} \text{ A/V}^{3/2}$, a beam voltage of 1100 V, a discharge voltage of 25 V, and a discharge chamber electron temperature of 5 eV. The normalized perveance per hole (NPPH) is proportional to the ion current density and is defined in

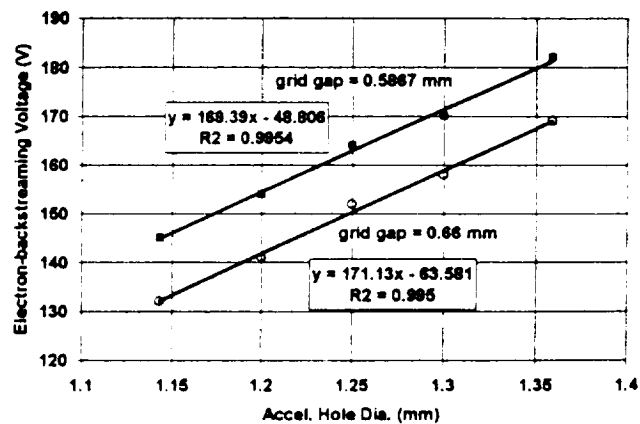


Fig. 8 The electron-backstreaming voltage is a linear function of the accelerator grid hole diameter.

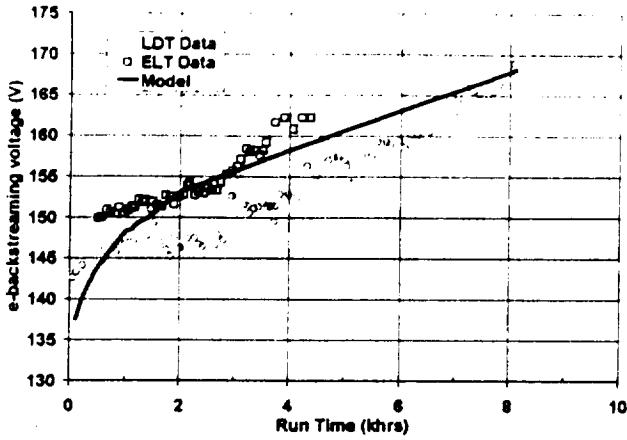


Fig. 11 Comparison of the electron-backstreaming model with data from the 8,000-hr LDT and the ongoing ELT.

backstreaming voltage as a function of time for conditions corresponding to the 8,000-hr and ELT tests. Comparison of the model with the electron-backstreaming data from these tests [33,42] is given in Fig. 11 for a grid gap of 0.66 mm. The data in this figure indicates that the model slightly under predicts the slope of the electron-backstreaming variation with time. Thus, the model is optimistic when extrapolated to longer times. In addition, it shows that the transient associated with the removal of the cusps lasts approximately 2,000 hours.

The model can be recast to calculate the time required to reach the onset of electron-backstreaming. This time is given as,

$$T_{eb} = (D^2 - d_0^2) \left(\frac{\pi \rho t_a e f_a N_h}{4 J_b \alpha_a Y m_g (1 - \beta) \lambda_h} \right) \quad (6)$$

where,

$$D = \frac{V_a - 1209 l_g^2 + 1675 l_g - 520.5}{166.7} \quad (7)$$

represents the hole diameter at which electron-backstreaming occurs for an accelerator voltage of V_a . The actual time to the onset of electron-backstreaming is given by Eq. (6) plus the time required to remove the cusps (approximately 2,000 hours). The values or ranges of values for the parameters in Eqs. 6 and 7 are given in Tables 3 and 4. In these equations, the

Table 4 Parameters for Eqs. (3)-(7)

Symbol	Definition	Values
d_h	Accelerator grid hole diameter after the cusp has been removed [m]	1.27×10^{-3}
l_g	Screen-Accelerator grid gap [m]	5.9×10^{-4} to 6.6×10^{-4}
N_h	Number of holes in the accelerator grid	15,400
T	Run Time [s]	
λ_h	Sputter yield parameter for hole erosion	0.5 to 1.0
ρ	Density of accelerator grid material [kg/m^3]	10220

parameters f_a and l_g affect the erosion geometry, while the parameters β and λ_h affect the erosion rate. The allowable ranges of values for f_a , β and λ_h result in possible values for $(1 - \beta) \lambda_h / f_a$ that can be approximately a factor of two greater than or less than that given in Eq. (5). In addition, the allowable values of β and λ_h permit a factor of three variation in the erosion rate of the accelerator grid holes.

With these values a Monte Carlo simulation, assuming a constant accelerator grid voltage of -180 V, results in the failure risk shown as the left-most curve in Fig. 12. This curve shows that there is a very high probability that electron-backstreaming will occur before 16,000 hours of operation at full power. Indeed, there is a 50% chance that it will occur at 10,000 hours. The calculated distribution of total mass loss rates from the holes is given in Fig. 13. The mass loss rate from the holes in the 8,000-hr test was estimated to be approximately 1.1 g/khr [42]. The higher erosion rates calculated in the simulation result from the lack of knowledge regarding the allowable values of some of the key parameters. As before, this lack of knowledge shows up as an increased failure risk.

To delay the onset of electron backstreaming, the magnitude of the accelerator voltage could be increased. The NSTAR PPU has the capability to operate with an accelerator grid voltage as negative as -250 V. Rerunning the Monte Carlo simulation with the accelerator grid voltage fixed at this level results in the middle curve in Fig. 12. This change has increased the B1 life from about 5,000 hours to approximately 16,000 hours. Clearly, the beneficial effect of making the accelerator grid more negative outweighs the increased erosion rate associated with the greater

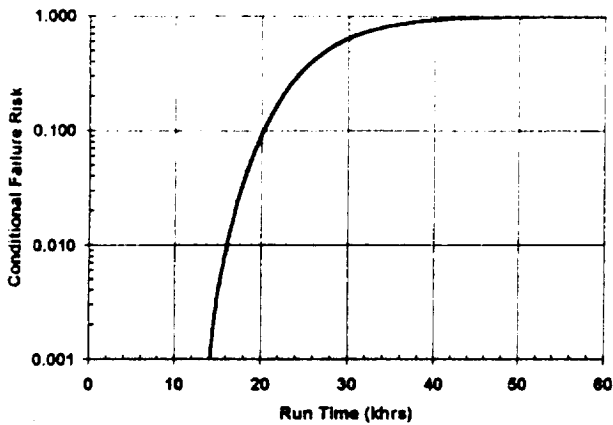


Fig. 14 Accelerator grid failure risk for the combined failure modes of electron-backstreaming and structural failure due to erosion on the downstream surface of the grid.

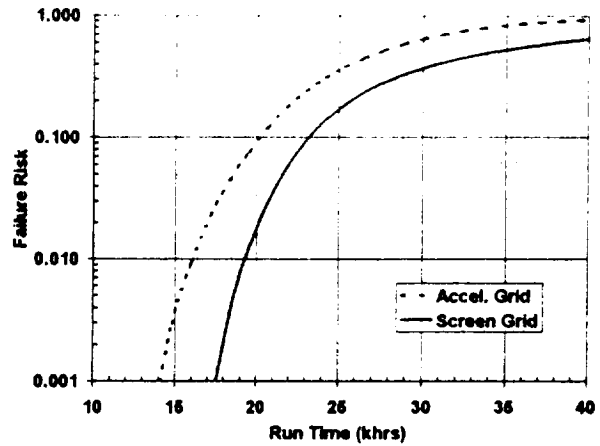


Fig. 16 Comparison of screen grid and accelerator grid failure risks.

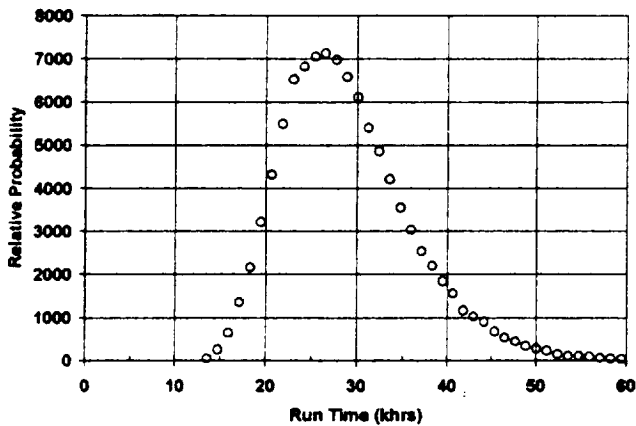


Fig. 15 Accelerator grid failure distribution for the combined failure modes.

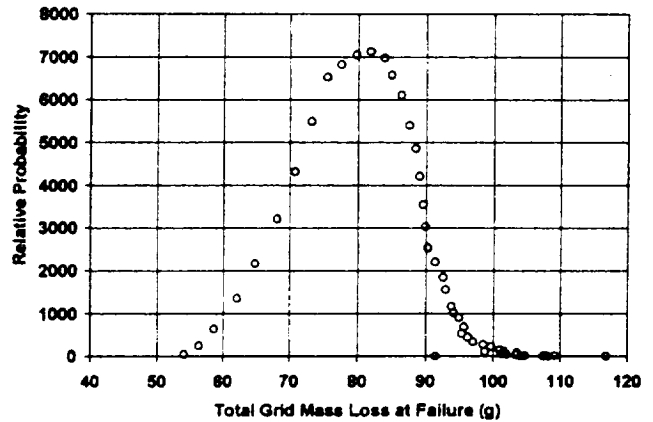


Fig. 17 Calculated distribution of total mass lost from the accelerator grid at failure for the combined failure modes.

for operation at full power which is the most stressing case. Therefore, even though the lower slope exhibited by the model in Fig. 11 may make the electron-backstreaming model slightly optimistic the conservatism implied by considering only full power operation is believed to result in the overall model still being conservative

Finally, the total calculated mass loss from the accelerator grid at failure (either structurally or from electron-backstreaming) is given in Fig. 17. The most probable value corresponds to a mass loss of approximately 80 g.

Conclusions

Ion propulsion is an enabling technology for the ST4/Champollion comet lander mission in the sense that it makes the mission affordable. The ST4 ion propulsion system is a three-engine version of the NSTAR hardware that is currently flying on DS1. This system will carry 385 kg of xenon to provide a ΔV of 11.4 km/s. Mass and cost constraints place a high premium on being able to accomplish this mission with only three NSTAR ion engines. This requires that the engines be capable of processing approximately 160 kg

- presented at the IAA International Conference on Low-Cost Planetary Missions, April 12-15, 1994.
19. Sauer, C. G. and Yen, C. L., "Planetary Mission Capability of Small Low Power Solar Electric Propulsion Systems," IAA-L-0706, presented at the IAA International Conference on Low-Cost Planetary Missions, April 12-15, 1994.
 20. Sauer, C. G., "Solar Electric Performance for Medlite and Delta Class Planetary Missions," AAS 97-726, presented at the AAS/AIAA Astrodyamics Specialist Conference, Aug. 4-7, 1997.
 21. <http://www.estec.esa.nl/spdwww/rosetta/html/main.html>
 22. Polk, J. E., et al., "In-Flight Validation of the NSTAR Ion Thruster Technology on the Deep Space One Mission," AIAA-99-2274, presented at the 35th AIAA/ASME/SAE/ASEE Joint Propulsion Conference, June 21-23, 1999.
 23. Ganapathi, G. B. and Engelbrecht, C. S., "Post-Launch Performance Characterization of the Xenon Feed System on Deep Space One," AIAA99-2273, presented at the 35th AIAA/ASME/SAE/ASEE Joint Propulsion Conference, June 21-23, 1999.
 24. Rawlin, V. K., et al., "NSTAR Flight Thruster Qualification Testing," AIAA-98-3936, presented at the 34th AIAA/ASME/SAE/ASEE Joint Propulsion Conference, July 6-9, 1998.
 25. Sovey, J., et al., "Development of an Ion Thruster and Power Processor for New Millennium's Deep Space 1 Mission," AIAA-97-2778, Dec. 1997.
 26. Pawlik, E. V., "An Experimental Evaluation of Array of Three Electron-Bombardment Ion Thrusters," NASA TN D-2597, January, 1965.
 27. Pawlik, E. V. and Reader, P. D., "Accelerator Grid Durability Tests of Mercury Electron-Bombardment Ion Thrusters," NASA TN D-4054, July, 1967.
 28. Masek, T. D., "Solar Electric Propulsion Thrust Subsystem Development," Technical Report 32-1579, Jet Propulsion Laboratory, California Institute of Technology, March 15, 1973.
 29. Rawlin, V. K. and Manteniaks, M. A., "A Multiple Thruster Array for 30-cm Thrusters," AIAA Paper No. 75-402, March 19-21, 1975.
 30. Fitzgerald, D. J., "Factors in the Design of Spacecraft Utilizing Multiple Electric Thrusters," AIAA Paper No. 75-404, March 19-21, 1975.
 31. Lathem, W. C., "Particle and Field Measurements on Two J-Series 30-Centimeter Thrusters," NASA Technical Memorandum 81741, April, 1981.
 32. Tierney, C. M., Brophy, J. R., and Mueller, J., "Plume Characteristics of a Multiple Ion Source Thruster," AIAA-95-3067, July 10-12, 1995.
 33. Anderson, J. R., et al., "Results of an Ongoing Long Duration Ground Test of the DS1 Flight Spare Engine," AIAA-99-2875, presented at the 35th AIAA/ASME/SAE/ASEE Joint Propulsion Conference, June 21-23, 1999.
 34. Polk, J. E., et al., "Probabilistic Analyses of Ion Engine Accelerator Grid Life," IEPC-93-176, presented at the 23rd International Electric Propulsion Conference, Seattle, WA, Sept. 1993.
 35. Polk, J. E., Brophy, J. R., and Wang, J., "Spatial and Temporal Distribution of Ion Engine Accelerator Grid Erosion," AIAA-95-2924, presented at the 31st AIAA/ASME/SAE/ASEE Joint Propulsion Conference, July, 1995.
 36. Patterson, M. J., et al., "2.3 kW Ion Thruster Wear Test," AIAA-95-2516, presented at the 31st AIAA/ASME/SAE/ASEE Joint Propulsion Conference, July, 1995.
 37. Polk, J. E., et al., "A 1000-Hour Wear Test of the NASA NSTAR Ion Thruster," AIAA-96-2717, presented at the 32nd AIAA/ASME/SAE/ASEE Joint Propulsion Conference, July, 1996.
 38. Brophy, J. R., Polk, J. E., and Rawlin, V. K., "Ion Engine Service Life Valication by Analysis and Testing," AIAA-96-2715, presented at the 32nd AIAA/ASME/SAE/ASEE Joint Propulsion Conference, July, 1996.
 39. Polk, J. E., et al., "The Effect of Engine Wear on Performance in the NSTAR 8000 Hour Ion Engine Endurance Test," AIAA-97-3387, presented at the 33rd AIAA/ASME/SAE/ASEE Joint Propulsion Conference, July, 1996.
 40. Polk, J. E., et al., "In Situ, Time-Resolved Accelerator Grid Erosion Measurements in the NSTAR 8000 Hour Ion Engine Wear Test," IEPC-97-047, presented at the 25th International Electric Propulsion Conference, Aug. 1997.
 41. Anderson, J. R., Polk, J. E., and Brophy, J. R., "Service Life Assessment for Ion Engines," IEPC-97-049, presented at the 25th International Electric Propulsion Conference, Aug. 1997.
 42. Polk, J. E., et al., "An 8200 Hour Wear Test on the NSTAR Ion Thruster," AIAA-99-2446, presented at the 35th AIAA/ASME/SAE/ASEE Joint Propulsion Conference, June 21-23, 1999.
 43. Zakany, J. S. and Pinero, L. R., "Space Station Cathode Ignition Test Status at 32,000 Cycles,"